Bulgarian Journal of Physics vol. **XX** (20XX) 1–9

# Shadow of Rotating Wormhole with Global Monopole Charge

**Radostina Z. Zheleva**[1*], **Galin N. Gyulchev**[2]
[1]Institute of Astronomy and National Astronomical Observatory, Bulgarian Academy of Sciences, 1784 Sofia, Bulgaria
[2]Department of Theoretical Physics, Faculty of Physics, Sofia University, Sofia 1164, Bulgaria
[*]Corresponding author Email: rzheleva@astro.bas.bg

Received *17 November 2024*

**Abstract.** This paper explores the shadows cast by a rotating, traversable wormhole, specifically the topologically charged Schwarzschild–Klinkahmer (SK) wormhole spacetime. We derive the equation of motion for photons, implement a numerical ray-tracing algorithm based on the Hamiltonian equation, and visualize the shadows produced by this rotating wormhole for an observer located at specified Boyer-Lindquist coordinates within the domain of outer communication. Additionally, we present visualizations of the shadows for various values of the metric parameters and compare our findings with those obtained in the Kerr case.

KEY WORDS: Rotating Wormholes, Global monopole, Shadows, Geodesics, Effective potential.

## 1 Introduction

One of the most important phenomenological and observational characteristics of wormholes is their shadow. Currently, we are witnessing one of the most significant observational confirmations of the existence of black holes, beginning with the Event Horizon Telescope's capture of the first image of a black hole's shadow in the M87 galaxy (April 10, 2019). Later, in 2022, it also provided an image of Sgr A, the central supermassive black hole at the heart of our galaxy [1, 2]. The specific characteristics, such as the size and shape of these shadows, can be used to extract information about the physical properties of both event-horizon objects, such as black holes, and exotic objects, such as traversable wormholes. We can estimate their mass, spin, and multipole moments, as well as distinguish between different gravitational theories [3]. Since shadows are not restricted to objects with event horizons, we can investigate the shadow silhouettes of horizonless objects by examining light propagation near the photon regions of naked singularities or wormholes.

We consider a stationary, rotating traversable wormhole in the presence of a topological defect produced by a global monopole charge. Such defects, including global monopole charges and cosmic strings, are believed to arise during phase transitions in the early universe [4]. Recent studies have discussed the existence of a wormhole in the bulge and halo of the Milky Way galaxy (MWG) with a global monopole charge [5]. The stability of these wormholes, characterized by a MacMillan DM profile in the MWG bulge, was explored in [6, 7]. Additional research has focused on black holes with global monopole charges [8, 9], as well as various aspects of Hawking radiation, thermodynamic stability, and gravitational lensing in such spacetime [10–12]. The gravitational lensing of non-rotating Schwarzschild-Klinkahmer (SK) wormhole spacetime was investigated in [13]. Observational features of global monopole black holes were studied in [14]. Moreover, a comprehensive review of the shadows cast by compact objects can be found in [15].

This paper examines photon motion and circular orbits around a topologically charged rotating (TCR) wormhole and its shadows. The paper is organized as follows: Section 2 introduces the topologically charged Schwarzschild–Klinkahmer (SK) wormhole spacetime. Section 3 briefly discusses geodesic motion in this spacetime. Section 4 focuses on the shapes of the shadows of rotating wormholes for varying spin, global monopole, and throat parameters. We conclude with some comments and observations.

## 2 Topologically Charged Rotating Wormhole

In this section, we consider the rotating generalization of the four-dimensional topologically charged Schwarzschild–Klinkhamer wormhole metric, which is a non-vacuum solution to the Einstein field equations. The topologically charged metric of the rotating wormhole, expressed in Boyer—Lindquist coordinates, is stationary and axially symmetric, and is described by the line element [16]:

$$\begin{aligned} ds^2 &= g_{tt}\,dt^2 + g_{\xi\xi}\,d\xi^2 + g_{\theta\theta}\,d\theta^2 + 2\,g_{t\phi}\,dt\,d\phi + g_{\phi\phi}\,d\phi^2 \qquad (1)\\ &= -A\,dt^2 + B\left(1+\frac{b^2}{\xi^2}\right)^{-1}\frac{d\xi^2}{\alpha^2} + \Lambda\,d\theta^2 - 2\,H\,dt\,d\phi + K\,\sin^2\theta\,d\phi^2, \end{aligned}$$

with

$$\begin{aligned} A &= \left(1-\frac{2\,M\sqrt{\xi^2+b^2}}{\Lambda}\right), \quad B = \frac{\xi^2+b^2+a^2\,\cos^2\theta}{\Delta},\\ H &= \frac{2\,M\,a\sqrt{\xi^2+b^2}\,\sin^2\theta}{\Lambda}, \quad \Lambda = \xi^2+b^2+a^2\,\cos^2\theta,\\ K &= \xi^2+b^2+a^2+\frac{2\,M\,a^2\sqrt{\xi^2+b^2}\,\sin^2\theta}{\Lambda},\\ \Delta &= \xi^2+b^2+a^2-2\,M\sqrt{\xi^2+b^2}, \qquad (2) \end{aligned}$$

where $0 < \alpha < 1$ is the global monopole charge parameter, $M \neq 0$ represents the mass of the objects, $a = J/M$ represents spin angular momentum per unit mass, and the parameter $b$ is strictly positive and non-zero, with $b > 2\,M$. In the specific case $a = 0$, this metric (Eq. 1) reduces to a topologically charged non-rotating SK-wormhole spacetime, discussed in details in Ref. [13]. The coordinates are in the ranges

$$-\infty < t < +\infty, \quad -\infty < \xi < +\infty, \quad 0 < \theta < \pi, \quad 0 \leq \phi < 2\,\pi. \tag{3}$$

The wormhole's throat lies at $\xi_{th} = 0$. The coordinate $\xi = \xi(r)$ is related to the standard Boyer–Lindquist coordinate $r$ via the transformation $r^2 = \xi^2 + b^2$, i.e. the wormhole's throat radius is $r_{th} = b$.

## 3 Geodesic Motion

### 3.1 Geodesic equations

The spacetime of rotating, topologically charged rotating wormhole is characterized by four constants of motion: the Lagrangian $\mathcal{L}$, energy $E$, angular momentum $L_z$ and the Carter constant $K$. It also admits two Killing vectors, $k_1 = \partial_t,\ k_2 = \partial_\varphi$, which ensure conservation of $E$ and $L_z$.

In the present analysis, we apply the Hamilton–Jacobi method, to derive the equations of motion in the geometry of the topologically charged rotating SK-wormhole. We decouple the radial ($\xi$) and angular ($\theta$) components of the Hamilton–Jacobi equation and express all the equations of motion for a test particle in the given geometry. For this purpose, we introduce the Hamilton–Jacobi equation

$$\frac{\partial S}{\partial \tau} + \frac{1}{2} g^{\mu\nu} \frac{\partial S}{\partial x^\mu} \frac{\partial S}{\partial x^\nu} = 0, \tag{4}$$

$$S = -\frac{1}{2}\mu^2 \tau - Et + L_z \varphi + f(\xi, \theta) \tag{5}$$

where $f(\xi, \theta)$ is a function of the variables $\xi$ and $\theta$, the constants of motion $\mu$, $E$, and $L_z$ denote the mass, the energy and the angular momentum of the particle respectively. Furthermore, the separability of the Hamilton-Jacobi equation in topologically charged wormhole space-time implies that $f(\xi, \theta)$ can be expressed as a sum of two different functions which only depend on $\xi$ and $\theta$ independently, i.e.

$$f(\xi, \theta) = S_\xi(\xi) + S_\theta(\theta). \tag{6}$$

The substitution of (6) together with the metric components $g^{\mu\nu}$ and into Hamilton-Jacobi equation results in two first order ordinary differential equations. Using the expression for the canonical momenta $P_\mu$ given by

$$P_\mu = \frac{\partial S}{\partial x^\mu} \tag{7}$$

and identifying

$$P_t = -E, \qquad P_\varphi = L_z, \tag{8}$$

along with $g_{\mu\nu}\dot{x}^\mu\dot{x}^\nu = \epsilon\,\mu^2$, where $\epsilon = -1, 0$ for timelike and null geodesics respectively, we can derive separate equations for the radial $\xi$ and $\theta$ motion:

$$\frac{1}{\alpha}\left(1+\frac{b^2}{\xi^2}\right)^{-1/2}\Lambda\,\frac{d\xi}{d\tau} = \pm\sqrt{R(\xi)}, \tag{9}$$

$$\Lambda\frac{d\theta}{d\tau} = \pm\sqrt{\Theta(\theta)}. \tag{10}$$

Although there are three constants of motion $E$, $L$, and $Q$, the geodesic motion of a photon is characterized by two independent parameters defined as the impact parameters:

$$\eta = \frac{L}{E}, \quad \beta = \frac{Q}{E^2}. \tag{11}$$

These parameters, along with a new affine parameter $\tilde{\tau} = E\tau$, eliminate the energy $E$ from the geodesic equations, thereby parameterizing the photon motion solely by $\beta$ and $\eta$. In terms of these impact parameters, the functions $R(r)$ and $\Theta(\theta)$ are expressed as:

$$\mathcal{R}(\xi) = \frac{R(\xi)}{E^2} = (a^2+\xi^2+b^2-a\beta)^2 - \Delta(\eta+(a-\beta)^2+\mu^2(\xi^2+b^2)), \tag{12}$$

$$\mathcal{T}(\theta) = \frac{\Theta(\theta)}{E^2} = \beta + \cos^2\theta\left(a^2(1-\mu^2) - \frac{\eta^2}{\sin^2\theta}\right), \tag{13}$$

where $\mu = 0$ for a photon. Once these equations are solved, the other two variables can be obtained by integrating the first-order equations. In terms of the impact parameters, these equations are expressed as

$$\Lambda\frac{dt}{d\tau} = \frac{(a^2+b^2+\xi^2)^2 - \Delta\,a^2\sin^2\theta}{\Delta} - \eta\,\frac{2aM\sqrt{\xi^2+b^2}}{\Delta}, \tag{14}$$

$$\Lambda\frac{d\varphi}{d\tau} = \frac{2aM\sqrt{\xi^2+b^2}}{\Delta} + \eta\,\frac{\Delta - a^2\sin^2\theta}{\sin^2\theta}. \tag{15}$$

Thus, we derive the equations describing null geodesics in the spacetime of a topologically charged traversable wormhole. Utilizing the radial equation of motion, we define the effective potential for photons. By maximizing the effective potential, we identify families of unstable spherical orbits. This process results in two quadratic equations involving the impact parameters and the radial position of the unstable spherical orbit. These equations establish a relationship between the impact parameters that must be satisfied at the boundary of the shadow [15].

## 4 Shadow of Topologically Charged Wormhole

To calculate the shadow of the wormhole, we first derive the effective potential for photons and establish the conditions for its maximum, which are associated with a family of unstable spherical photon orbits defined by the following equations:

$$V_{\text{eff}} = 1, \qquad \frac{V_{\text{eff}}}{d\xi} = 0, \qquad \frac{d^2 V_{\text{eff}}}{d\xi^2} \leq 0. \tag{16}$$

The radial geodesic equation can be expressed as one-dimensional motion within an effective potential defined as:

$$\left(\frac{d\xi}{d\tilde{\tau}}\right)^2 + V_{\text{eff}} = 1, \quad V_{\text{eff}} = 1 - \frac{\alpha^2}{\Lambda^2}\left(1 + \frac{b^2}{\xi^2}\right)\mathcal{R}(\xi). \tag{17}$$

We can define the second derivative of the effective potential at the maximum, in the following way:

$$\frac{d^2 V_{\text{eff}}}{d\xi^2} = -\frac{\alpha^2}{\Lambda^2}\left(1 + \frac{b^2}{\xi^2}\right)\frac{d^2\mathcal{R}}{d\xi^2}. \tag{18}$$

We can determine the set of the unstable circular photon orbits that define a curve in parameter space $(\eta, \beta)$, which corresponds to the shape of the shadow. The conditions for these orbits, expressed in terms of the function $R(\xi)$ are:

$$\mathcal{R}(\xi) = 0, \qquad \frac{d\mathcal{R}}{d\xi} = 0, \qquad \frac{d^2\mathcal{R}}{d\xi^2} \geq 0. \tag{19}$$

Thus, we obtain two algebraic equations, that provide the connections between the impact parameters $\eta$ and $\beta$ and the variable $\xi$:

$$\eta = -\frac{(b^2+\xi^2)^{3/2} - 3M(b^2+\xi^2) + a^2\sqrt{\xi^2+b^2} + Ma^2}{a(\sqrt{\xi^2+b^2} - M)}, \tag{20}$$

$$\beta = -\frac{(b^2+\xi^2)^{3/2}[(b^2+\xi^2)^{3/2} - 6M(b^2+\xi^2) + 9M^2\sqrt{\xi^2+b^2} - 4Ma^2]}{a^2(\sqrt{\xi^2+b^2} - M)^2} \tag{21}$$

A second family of unstable spherical photon orbits arises from the maximum of the effective potential at the wormhole's throat. In this case, the metric function $g^{\xi\xi}$ vanishes. The photon orbits in this family are radially fixed at the throat, $\xi = \xi_{th}$. The equations describing this family are:

$$\Delta(\xi) = 0, \qquad \mathcal{R}(\xi) = 0, \qquad \frac{d\mathcal{R}}{d\xi} \geq 0. \tag{22}$$

The system of equations yield an implicit relation between the impact parameters $\eta$ and $\beta$.

We conduct a backward numerical ray tracing of light rays, starting from the observer's screen and ending at the wormhole's throat, $\xi = \xi_{th} = 0$. The null geodesic equations are expressed in Hamiltonian form and solved numerically. A photon's trajectory is projected onto the observer's plane using two angles, $\gamma$ and $\delta$, which are related to the 4-momentum of the photon via the impact parameters at the observer's location, as described in [17]:

$$x = -\xi_{obs} \tan\delta, \quad y = \xi_{obs} \sin\gamma. \tag{23}$$

To study the gravitational lensing patterns within the shadow, the wormhole's throat is divided into four quadrants, each assigned a unique color based on the angles $\theta_{cel}$ and $\phi_{cel}$. A grid of thin black lines, spaced $10^\circ$ apart, illustrates the distortion of these patterns. The color scheme is as follows: for the upper hemisphere of the throat, green represents $0 < \phi_{cel} < \pi$ and red for $\pi < \phi_{cel} < 2\pi$; for the lower hemisphere, blue covers $0 < \phi_{cel} < \pi$ and yellow covers $\pi < \phi_{cel} < 2\pi$.

## 5 Conclusions

To compare the distinctive features of the wormhole's shadow for different metric parameters, Figure 1 shows the apparent images of the Kerr black hole and a topologically charged rotating wormhole in the observer's plane $(x, y)$ for various values of the spin parameter $a/M$ and the global monopole charge $\alpha$, with a fixed wormhole throat radius $b = 2.5M$. The shadow of the TCR wormhole resembles that of the Kerr black hole for small spin values, but when the Kerr black hole approaches near-extremal spin ($a/M = 0.999$), the wormhole's shadow becomes more elongated than that of the Kerr black hole. The global monopole parameter $\alpha$ has a negligible effect on the size of the TCR wormhole's shadow.

Furthermore, Figure 2 illustrates the shadows of the TCR wormhole for different spin and global monopole parameters. In these cases, the wormhole's shadow becomes significantly more elongated for higher spin values, exceeding even the near-extremal Kerr black hole's angular momentum. Thus, over-rotating wormholes could exhibit highly elongated shadows at high angular momentum, differing dramatically from the Kerr black hole's shadow.

## Acknowledgements

The authors would like to express their gratitude to S. Pacheva and P. Nedialkov for their invaluable comments and discussions.

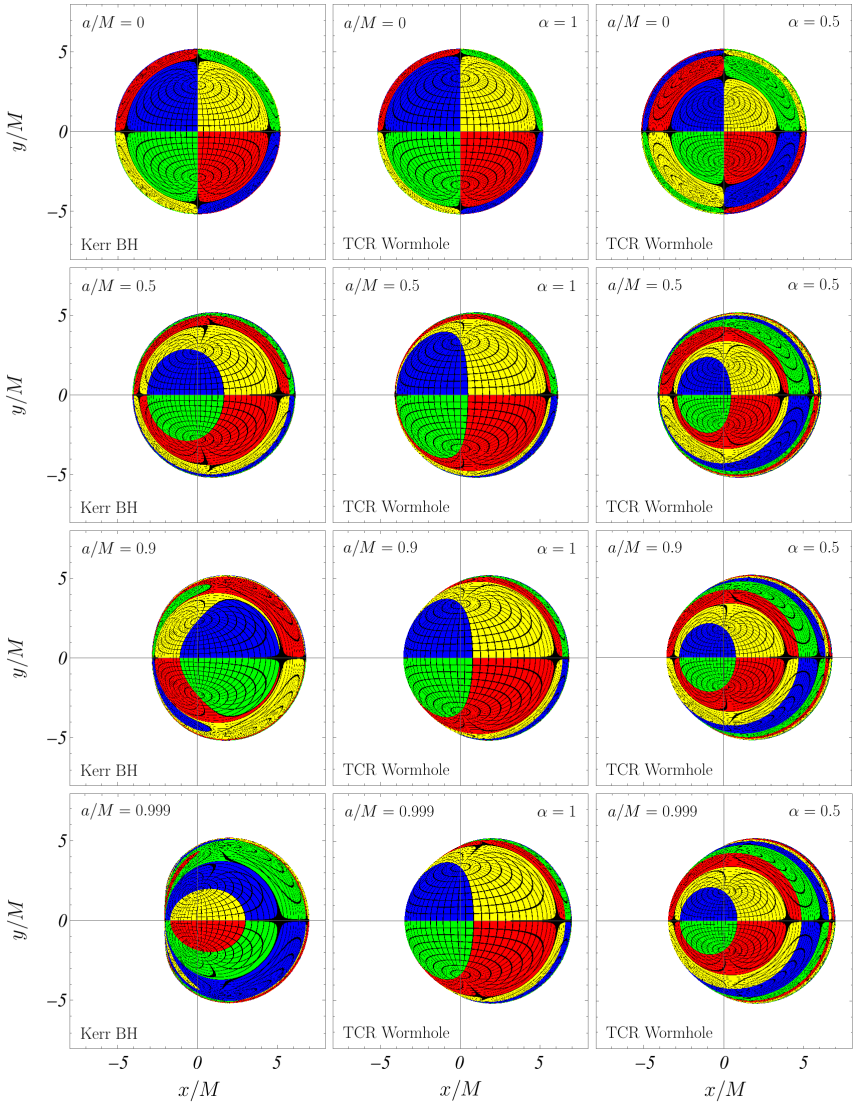


Figure 1. Comparison between the shadows of Kerr black holes and those of topologically charged rotating wormholes for different values of the spin parameter $a/M$ and the global monopole parameter $\alpha$. The set of colors represents the image of the wormhole's throat projected into the shadows. Parametrizing the throat with radius $r = b = 2.5M$ (or $\xi_{th} = 0$), azimuthal angle $\phi$ and polar angle $\theta$ the colours are defined as follows: $0 < \theta < \pi/2$ and $0 < \phi < \pi$ (*yellow*); $0 < \theta < \pi/2$ and $\pi < \phi < 2\pi$ (*blue*); $\pi/2 < \theta < \pi$ and $0 < \phi < \pi$ (*red*); $\pi/2 < \theta < \pi$ and $\pi < \phi < 2\pi$ (*green*).

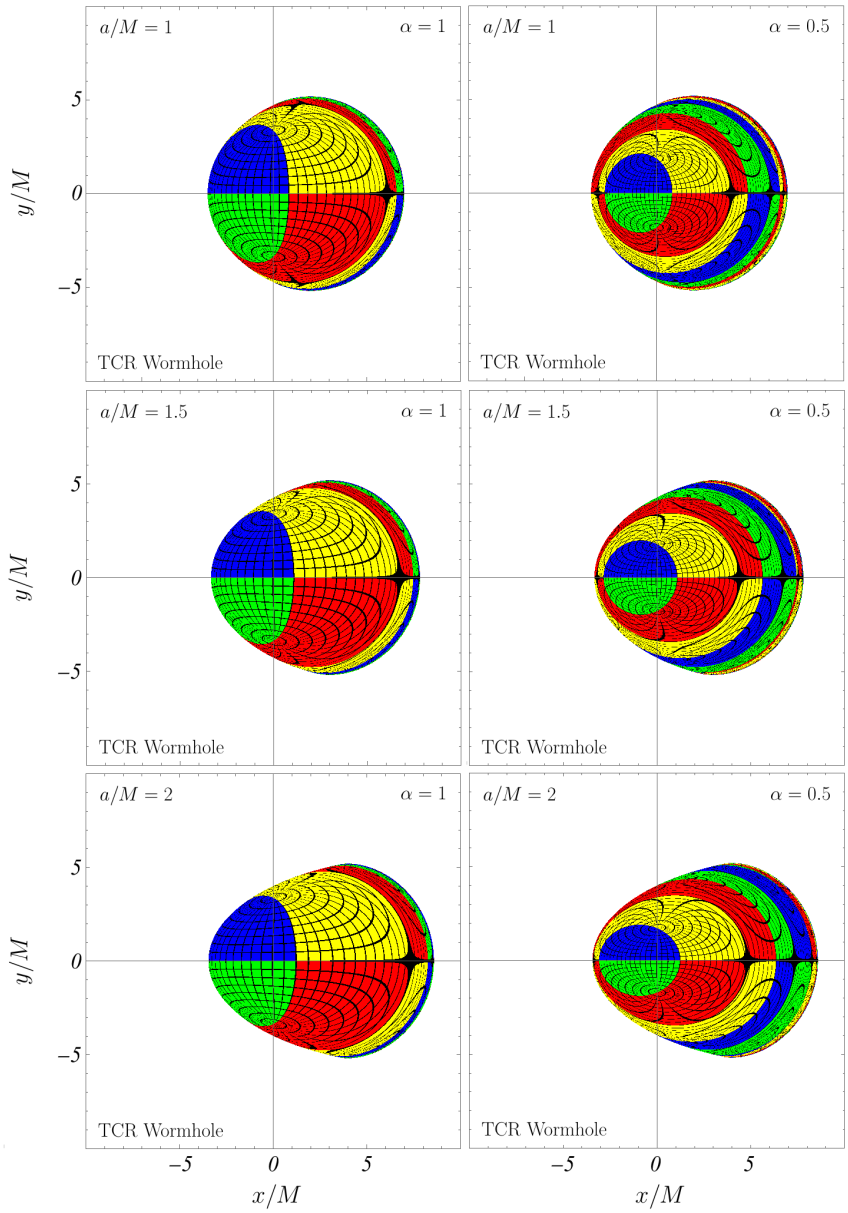


Figure 2. Examples of Topologically Charged Rotating Wormhole's shadows for different values of the spin parameter $a/M$ and global monopole parameter $\alpha$. The color scheme representing the image of the wormhole's throat projected into the shadow is the same as that in Figure 1.

## Bibliography


[1] E.H.T. Collaboration et al. (2019) First M87 Event Horizon Telescope Results. IV. Imaging the Central Supermassive Black Hole. *Astrophys. J. Lett.* **875** 1.

[2] E.H.T. Collaboration et al. (2022) First Sagittarius A* Event Horizon Telescope Results. II. EHT and Multiwavelength Observations, Data Processing, and Calibration. *Astrophys. J. Lett.* **930**(2) id L13, 31pp.

[3] G. Gyulchev, P. Nedkova, V. Tinchev, S. Yazadjiev (2019) Cusp structure in shadows casted by rotating wormholes. In: *AIP Conference Proceedings of 10th Jubilee International Conference of the Balkan Physical Union*, 26–30 August 2018, Sofia, Bulgaria. DOI: https://doi.org/10.1063/1.5091165

[4] R.H. Brandenberger (1994) Topological defects and structure formation. *Int. J. Mod. Phys. A* **09**(13) 2117-2189.

[5] M. Kalam, P. Das (2022) Wormhole in the Milky Way galaxy with global–monopole charge *Eur. Phys. J. C* **82** 342.

[6] K. Jusufi (2018) Conical Morris-Thorne wormholes with a global monopole charge. *Phys. Rev. D* **98** 044016.

[7] S. Sarkar, N. Sarkar, F. Rahaman (2020) Traversable wormholes in the bulge of Milky Way galaxy with Global Monopole Charge. *Eur. Phys. J. C* **80** 882.

[8] S. Haroon, K. Jusufi, M. Jamil (2020) Shadow images of a rotating dyonic black hole with a global monopole surrounded by perfect fluid. *Universe* **6**(2) 23.

[9] R. Karmakar, J.D. Gogoi, U. Dev Goswami (2023) Quasinormal modes and late time tails of perturbation fields on a Schwarzschild-like black hole with a global monopole in the Einstein-bumblebee theory. *Phys. Dark Univ.***41** 101249.

[10] F. Bento Lustosa, M. Emilia Xavier Guimarães, C. Nunes Ferreira, J. Lopes Neto, J. Abdalla Helayël-Neto (2019) On the Thermodynamical Black Hole Stability in the Space-Time of a Global Monopole in f(R)-Gravity. *J. High Energy Phys., Gravit. Cosmol.* **5**(3) July 2019.

[11] J. Xian, J. Zhang (2022) Deriving the Hawking Temperature of (Massive) Global Monopole Spacetime via a Topological Formula. *Entropy* **24**(5) 634.

[12] N. Dadhich, K. Narayan, U.A. Yajnik Schwarzschild black hole with global monopole charge. (1998) *Pranama – J. Phys* **50** 307-314.

[13] F. Ahmed (2023) Geodesics motion of test particles around Schwarzschild-Klinkhamer wormhole with topological defects and gravitational lensing. *J. Cosmol. Astropart. Phys.* **2023** November 2023..

[14] Guo-Ping Li, Ke-Jian He (2021) Observational appearances of a f(R) global monopole black hole illuminated by various accretions. *Eur. Phys. J. C* **81**(11) 1018.

[15] P. Nedkova (2023) Shadows and Accretion Disk Images of Compact Objects. In: *Lecture Notes in Physics* **1022** 67-99, Springer Cham.

[16] F. Ahmed Topologically Charged Rotating Wormhole (2023) *Acta Phys. Pol. B* **54** 11-A3.

[17] Pedro V.P. Cunha, Carlos A.R. Herdeiro, Eugen Radu, Helgi F. Rúnarsson (2015) Shadows of kerr black holes with scalar hair. *Phys. Rev. Lett.* **115**(21) 211102.